Experimental Femtosecond Photoionization of NaI

C. Jouvet,* S. Martrenchard, D. Solgadi, and C. Dedonder-Lardeux

Laboratoire de Photophysique Moléculaire du CNRS, Bât. 213, Université de Paris Sud, 91405 Orsay cedex, France

M. Mons, G. Grégoire, I. Dimicoli, F. Piuzzi, J. P. Visticot, J. M. Mestdagh, P. D'Oliveira, P. Meynadier, and M. Perdrix

DRECAM/SPAM, CEA Saclay, 91911 Gif/Yvette, France

Received: November 25, 1996; In Final Form: February 4, 1997[⊗]

Two-color two-photon femtosecond ionization experiments have been performed on NaI. The wave packet evolution of the A excited state has been followed by detecting photoions and photoelectrons. The results indicate that the Na^+ ions are formed when the wave packet is located at the outer turning point of the excited state. Surprisingly, the NaI^+ ions are also observed to be in phase with the Na^+ signal. Photoelectron spectra show that high kinetic energy electrons are produced when ionizing around the outer turning point, in agreement with the NaI^+ formation. The absence of signal corresponding to ionization from the covalent part of the excited state potential can only be understood if the absolute ionization cross section is much smaller in the covalent region of the A state (where the molecule can be considered as a van der Waals complex) than in the ionic $Na^+\cdots I^-$ part of the A state potential (where the interatomic distance is such that the ionization process may be considered as a photodetachment of the electron from I^- anion). Simulations taking into account that ionization occurs only when the wave packet is in the ionic region of the A state are in good agreement with experimental data.

Introduction

Extensive studies performed by the group of Zewail[1−9] have demonstrated that the NaI molecule is a benchmark for following wave packets evolution in the time domain. In their real time studies on this molecule, a first laser λ_1 prepares a wave packet in the first excited state of NaI ($\Omega = 0$) through the excitation of the X−A transition. The oscillations of the wave packet are followed by applying a second laser λ_2, delayed in time, which induces a transition to an upper state (corresponding to $Na(^2P) + I$). The result of these two excitations is observed through the fluorescence of the atomic sodium D line. When wave packet control is realized[4] a third laser is used to dump the wave packet toward the ground state. These studies have enabled characterization of the excited adiabatic A state potential (see Figure 1) as well as the upper state reached with the probe laser.

In many studies performed on neutral molecules, it has been demonstrated that wave packet oscillations can be followed by probing bound states (I_2,[10] Na_2,[11] Cs_2[12]) or neutral dissociative states such as in NaI[1−9] and Hg−Ar.[13] The probe can be achieved by photoionization. When photoionization is performed above the dissociation threshold of the ion, competition in time between simple ionization and dissociative ionization is expected. This has been observed in the case of Na_2[11] and the two processes are out-of-phase.

In the NaI case, theoretical studies have been published that simulate the time evolution of the predissociation using a femtosecond ionizing probe pulse and monitoring either the ion signal[14] or the photoelectron distribution[15] as a function of time.

The relevant potential energy curves are presented in Figure 1. In alkali halides, the ionic $Na^+I^-(X^1\Sigma_0^-)$ ground state crosses the covalent $\Omega = 0^-$ and $\Omega = 1$ excited states corresponding to the asymptotic $Na(^2S_{1/2}) + I(^2P_{3/2})$ limit. For symmetry reasons, only the $\Omega = 0^-$ state is coupled to the ground state. When the interaction is strong, as in NaI, a trapping well is formed, which is represented here by the adiabatic A state. An initial femtosecond pump pulse (λ_1) prepares the wave packet in the A state, and its evolution is followed through ionization to the NaI^+ state corresponding to the $Na^+ + I$ limit with a second femtosecond probe pulse (λ_2).

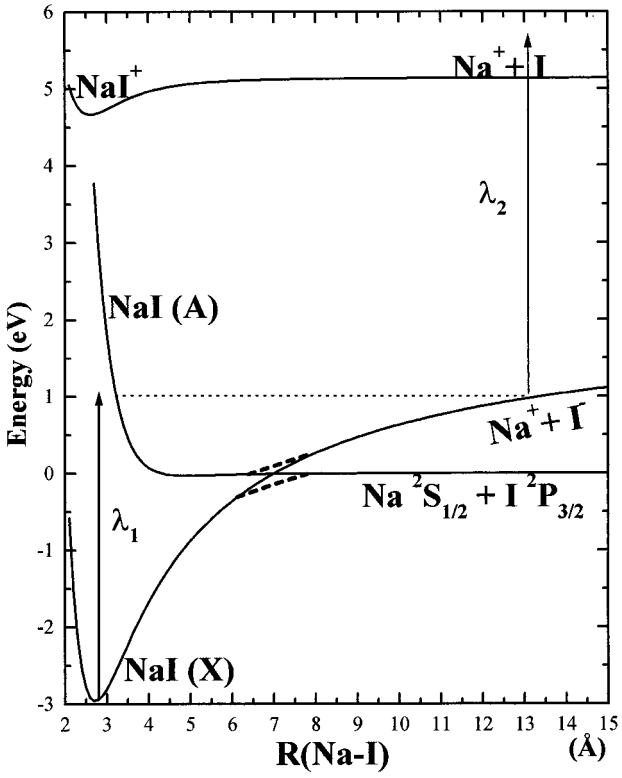

Figure 1. Potential energy curves of NaI from refs 7, 17, 18, and 19.

[⊗] Abstract published in *Advance ACS Abstracts,* March 1, 1997.

S1089-5639(96)03904-7 CCC: $14.00

In their work, Engel and Metiu[14] simulate both the excitation of the A state with a 300 nm femtosecond laser and the ionization with a short 4−5 eV photon and predict that monitoring the Na^+ or the NaI^+ signal should enable one to follow the wave packet dynamics in the A state. They also calculate that the Na^+ and NaI^+ ion signals should be out-of-phase, Na^+ being essentially formed from the ionic part of the A state potential, while NaI^+ should allow one to follow the wave packet in the inner covalent region of the potential.

Recently, Braun et al.[15] have calculated the time evolution of the photoelectron spectrum. This calculation predicts emission of an electron of high energy when the wave packet reaches the outer turning point of the excited A state and emission of a low-energy electron at the inner turning point.

In this paper, we present experimental results on the two-photon two-color femtosecond photoionization of NaI detecting the time evolution of both the mass spectrum and the photoelectron spectrum, which will enable us to test the theoretical predictions.[14,15] We will see that the results obtained here question the available theoretical predictions and call for a more refined treatment of the NaI ionization step as a function of the Na···I distance.

Experimental Section

The experimental setup consists of a supersonic beam coupled to a dual photoion photoelectron time-of-flight spectrometer and a femtosecond pump−probe laser.

The supersonic expansion that generates the beam is realized using a pulsed valve in the first chamber, which is evacuated by a 1500 L/s turbo pump. Since the valve cannot be heated at a sufficiently high temperature to get enough vapor pressure of NaI, an oven is added beyond the valve. Two types of ovens have been used so far. In the first case, the oven is located 1 cm downstream the valve and NaI is pushed by an argon flow into the ionization region of the mass spectrometer. Under this condition, the NaI temperature is the temperature of the oven, i.e., 600 °C. In the second setup, a small oven is attached to the valve and the helium gas passes through the oven heated at 450 °C before expansion through a 1 mm aperture hole. Under these conditions, the NaI is cooled in the expansion. No noticeable changes in the results have been seen with these two setups except that, in the latter case, an ion signal corresponding to Na_2I^+ has been observed in the mass spectrum.

The supersonic jet is skimmed before entering the extraction region of the double time-of-flight spectrometer. On one side, the electron time-of-flight is obtained by applying 1 V/cm in the extraction region and 2 V/cm in the acceleration region, the field-free path being 65 cm long. On the other side the ions are detected after a field-free region half a meter long. The two spectrometers cannot be operated at the same time. The ion or electron signals are detected with microchannel detectors, and the time-of-flight spectra are recorded on a digital oscilloscope interfaced to a PC computer.

The laser used in this experiment is the same as the one used in previous studies.[16] Briefly, the pump wavelength λ_1 in the 309−313 nm region is obtained by doubling the red light issued from a femtosecond dye laser with a 1 mm thick BBO crystal. The pulse energy is typically about 5 μJ, the spectral bandwidth is about 1 nm, and the temporal width is in the 120−175 fs range. Another pump wavelength domain, 345−348 nm, is obtained from mixing the ouput of the same red dye laser with the fundamental of a Ti:sapphire laser (pulse width, 130 fs) at 790 nm in a BBO crystal. The dye laser is not compressed after amplification, the temporal width being then 250−300 fs.

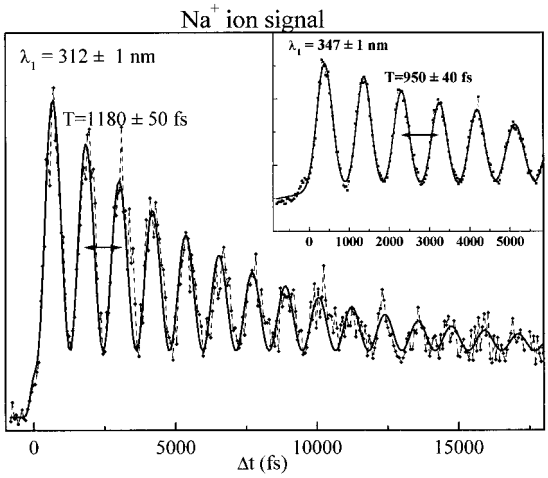

Figure 2. Na^+ ion signal as a function of the delay between pump (312 ± 1 nm) and probe lasers (263 nm). The period is 1180 ± 50 fs. In the insert, the pump laser wavelength is set at 347 nm. Under these conditions, the total energy is just enough to reach the $Na^+ + I$ ionic limit.

The probe wavelength λ_2 at 263 ± 1 nm is obtained by frequency tripling the light from the Ti:sapphire regenerative amplifier. The probe pulse is typically 150−200 fs wide, and the pulse energy is on the order of 30 μJ. The lasers are delayed in time by scanning a delay line at 33 fs steps. Both lasers are mildly focused in the beam between the grids of the spectrometer with 1 m lenses. A typical spectrum is obtained by averaging 10−20 scans with 25 laser shots per scan step.

Results

The signal observed for the Na^+ mass as a function of the delay between λ_1 and λ_2 is presented in Figure 2. The oscillations of the wave packet in the A state can be followed for more than 15 periods (18 ps) when $\lambda_1 = 312$ nm. In agreement with the results of the fully documented work of Rose et al.,[2] the period varies with the excitation wavelength: it drops from 1260 fs at 310 nm to 1180 fs at 312 nm (Figure 2) and 950 fs at 347 nm (Figure 2, insert).

The width of the oscillations (leading to an apparent background signal) also varies with the wavelength: the peak width is 320 ± 30 fs with the 347 nm excitation and 460 ± 50 fs with the 312 nm excitation, although the pump laser width is larger at 347 nm.

The time evolution of the two competing ionic channels Na^+ and NaI^+ and the zero-time determination are presented in Figure 3, where $\lambda_1 = 312$ nm and $\lambda_2 = 263$ nm. It is clear from the left part of Figure 3 that the recurrences of the A state wave packet are observed to be in phase for the two ions Na^+ and NaI^+ . The contrast of the oscillations is greater for NaI^+ than for Na^+; the peak width is 460 ± 50 fs for the Na^+ signal and 300 ± 30 fs for the NaI^+ signal. The maximum intensity is 10 times larger for Na^+ than for NaI^+.

The temporal overlap of the lasers ($t = 0$) has been measured in the following way. *p*-Xylene is added in the expansion, and λ_2 (263 nm) excites the molecule in its S_1 state. λ_1 (312 nm) ionizes the molecule when it arrives after λ_2. An increase in the ion signal is observed as the delay is scanned, which is the result of the convolution of the temporal width of the laser with an ionization step function and is presented in the upper right trace of Figure 3. From this curve, the convolution of the laser widths can be estimated to be 250 ± 30 fs, and the $t = 0$ time can be measured with an uncertainty of ±50 fs. Once time $t = 0$ is measured, we can see that the first peak appears with a 600 ± 50 fs delay.

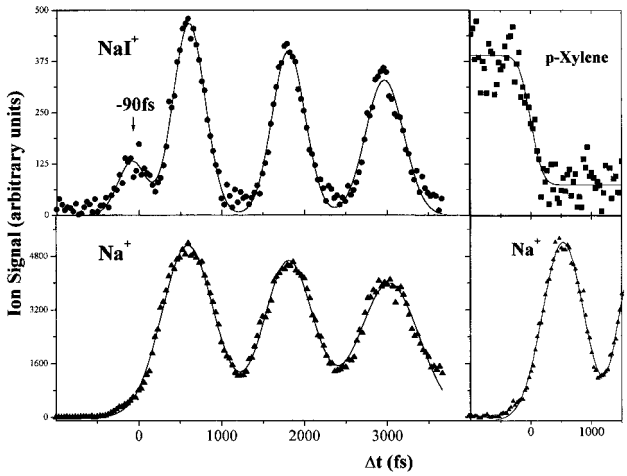

Figure 3. Ion signal as a function of delay between pump and probe laser: (upper left) NaI^+ ion signal as a function of the delay between the pump (263 nm) and the probe (312 nm) lasers; (lower left) Na^+ ion signal as a function of the delay between the pump and the probe lasers, where the peaks are fitted by Gaussian functions; (upper right) step function obtained on the *p*-xylene molecule; (lower right) Na^+ signal obtained in the same experiment.

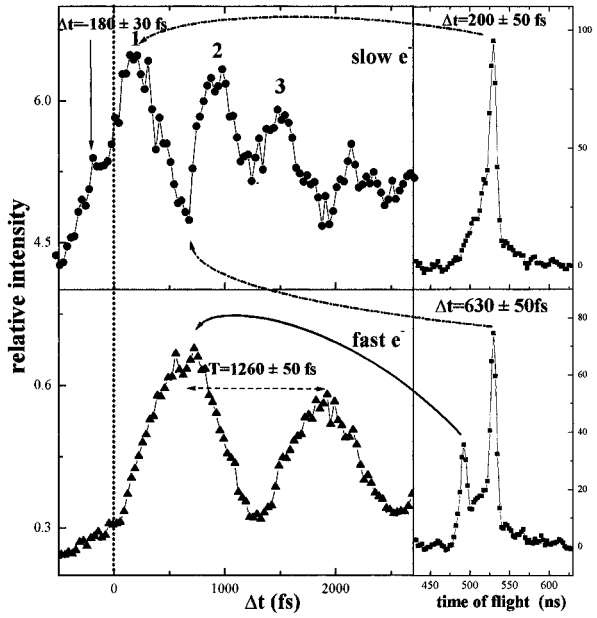

Figure 4. Photoelectron signal as a function of delay between pump and probe lasers. (Right) Photoelectron spectra recorded at fixed delay between pump (310 nm) and probe (263 nm) lasers (top, $\Delta t = 200$ fs; bottom, $\Delta t = 630$ fs). It should be noted that these spectra are not corrected for the detection efficiency of the spectrometer. Slow electrons detection is highly favored. Furthermore, one-color two-photon ionization with the 263 nm laser yields an important background of slow electrons that has not been subtracted. (Left) Time evolution of the electron signal as a function of the delay between pump (310 nm) and probe (263 nm) pulses where the background has been subtracted (upper curve, slow electrons 0−500 cm^{-1}; lower curve, fast electrons 2000−3400 cm^{-1}).

In Figure 3, a small peak at $\Delta t = -90 \pm 30$ fs can also be noticed on the NaI^+ channel. This peak does not gives rise to recurrences (at negative delays).

Figure 4 presents the results from detecting energy-resolved photoelectrons with $\lambda_1 = 310$ nm and $\lambda_2 = 263$ nm, which corresponds to a period of 1260 ± 50 fs. The photoelectron spectra recorded at two different delays are presented on the right side of Figure 4. When the delay is 630 fs, i.e., corresponding to the maximum ion signal, two peaks are clearly observed, the first one arriving between 480 and 500 ns and the second one between 520 and 540 ns. The first one can be calculated to correspond to fast electrons $2000 < E < 3400$ cm^{-1} and the second one to low-energy electrons $E < 500$ cm^{-1}. The time evolution of the photoelectron spectrum has been recorded by selecting two time-of-flight (or energy) regions in the photoelectron spectrum. The first region is centered on high-energy electrons (time-of-flight, 495 ns), and the second region centered at 530 ns monitors low-energy electrons. The two peaks are integrated, and their intensities are recorded as the delay between the probe and the pump lasers is changed.

In the right part of Figure 4, the lower trace presents the evolution of high-energy electrons. The oscillations are perfectly in phase with the signal observed for Na^+ and NaI^+. In contrast, the oscillations of the slow electrons (upper part in Figure 4) are at a minimum when the signal for the fast ones is a maximum. The first peak, labeled 1 in the figure, is delayed by 200 ± 40 fs from time $t = 0$, the second one (2) is delayed by 950 ± 50 fs, and the third one (3) is at 1500 ± 80 fs. These last two peaks are symmetrical with respect to the minimum of the ion and the fast electron signal, i.e., symmetrical with respect to the period.

Discussion

The present experimental results are discussed in light of previous studies by the group of Zewail.[1−9] A simple model is presented that explains the main features and is compared to more refined theoretical studies already published.[14,15]

First, we point out that the recurrences are observed in the photoionization study as predicted by the calculations of Engel et al.[14] Although the pump wavelength (312 ± 1 nm) for the experiment presented in Figure 1 is close to the one used by Cong et al. in ref 3 (310 nm), the oscillations we observe do not show the same trend; we do not observe a "chaotic" regime between 10 and 20 ps as they do. The oscillations smoothly decrease in the entire 0−20 ps region. This behavior can be understood in view of the work of Chapman and Child[20] who predict long-lived states in this spectral region, the lifetimes being strongly dependent on the exact wavelength. This effect has not been studied systematically in this paper. We must also mention that the presence of chirp of the laser pulses has not been checked in the present experiment, although Sterling et al.[21] have shown that chirped pulses could increase or shorten the coherence time of the observation. The recurrence periods are in agreement with those given in ref 2, the measured periods being 1260 ± 50 fs at an excitation wavelength of 310 ± 1 nm, 1180 ± 50 fs at 312 ± 1 nm, and 950 ± 40 fs at 347 ± 1 nm.

The important result in the ionization experiment is the appearance time of the first peak in the Na^+ ion signal. For $\lambda_1 = 312$ nm the first peak appears with a 600 fs delay, for $\lambda_1 = 310$ nm the delay is 630 fs, and it is 470 fs for $\lambda_1 = 347$ nm. In each case the delay corresponds to half the recurrence period. Therefore, the Na^+ ion signal is observed when the wave packet has reached the outer turning point of the A state.

The most surprising experimental result is that NaI^+ and Na^+ channels are observed in phase. Thus, NaI^+ is obtained when the wave packet is at the outer turning point, i.e., when the interatomic distance is ∼12 Å. This is at first glance somewhat unexpected, since at this distance the binding energy of NaI^+ is on the order of 20 cm^{-1} (this value is calculated with the potential used in the next paragraphs to model the NaI^+ ion), whereas the total excess energy is on the order of 3400 cm^{-1} when $\lambda_1 = 310$ nm and $\lambda_2 = 263$ nm. This behavior can be understood by looking at the time-resolved photoelectron energy spectrum (Figure 4). At delays corresponding to ionization from

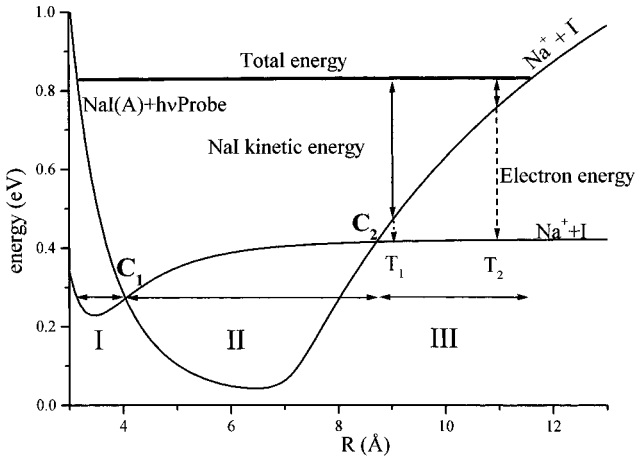

Figure 5. Scheme of the potential energy curves from refs 7, 17, 18, and 19. The excited adiabatic state potential taken from refs 7 and 17 has been shifted by the energy of the probe laser (4.714 eV)(dressed excited state). For the ionic NaI^+ potential, the long-range interaction that is the most important here is modeled with a $(\alpha_{Na^+} + \alpha_I)/(2R^4)$ term as usual for ion-neutral interaction, where α_{Na^+} and α_I are the Na^+ and I polarizabilities listed in ref 17. The repulsive part of the potential is modeled with an exponentially decreasing term adjusted to get a binding energy of .5 eV, and the short distance part of the potential is only indicative. The total energy corresponds to the energy in the A state plus the energy of the probe photon. It represents the total energy in the ionic state, including the potential energy and the kinetic energy of the nuclei and of the outgoing electron. In region I, the ionization process is energetically possible but not observed. In region II, the ionization is not possible because of the reflection principle. Ionization is only observed in region III.

the outer turning point, only very few low-energy electrons are emitted whereas the emission of high-energy electrons is at a maximum. Therefore, energy conservation implies that the internal energy content of the ion is minimal at the outer turning point, leading to the formation of stable NaI^+ ions together with Na^+ ions with low kinetic energy.

The scheme of the NaI potential curves relevant for this discussion is presented in Figure 5. The potential of the A state is issued from the work of Faist and Levine.[17] The potential for the ionic NaI^+ state is not known exactly; the long-range interaction, which is the most important here, is modeled with a $(\alpha_{Na^+} + \alpha_I)/(2R^4)$ term as usual for ion-neutral interaction, where α_{Na^+} and α_I are the Na^+ and I polarizabilities listed in ref 17. The repulsive part of the potential is modeled with an exponentially decreasing term adjusted to get a binding energy of .5 eV, and the short distance part of the potential is only indicative.

The observed results can be modeled with classical mechanics using a similar assumption as in refs 14 and 15, i.e., the dynamic reflection principle depicted in Figure 5, where the ionic NaI^+ potential and the excited A state potential shifted by the energy of the ionizing photon (4.714 eV) are plotted. If the A state potential, shifted by the laser energy, is lower than the ionic potential, no electron can be emitted. Thus, neither electrons nor ions should be detected for interatomic distances between 4 and 8.7 Å (between C1 and C2).

The kinetic energy of the outgoing electron is governed by the conservation of total energy and kinetic energy for the heavy particles; the ejection of the electron will not modify the nuclei kinetic energy ($E_{kinetic}$). Thus, the energy of the outgoing electron will just be the difference between the ionic NaI^+ potential and the excited A state potential shifted by the ionizing photon energy.

Two regions where ionization is possible can be distinguished in Figure 5. In region I around the inner turning point, the ionization process is energetically accessible. At the inner turning point, $E_{kinetic} = 0$, all the excess energy is removed by the electron, and NaI^+ ions should be produced. When the wave packet moves toward C1, $E_{kinetic}$ increases and the energy of the outgoing electron will accordingly decrease. Depending on the exact internuclear distance and binding energy in the NaI^+ ionic state, Na^+ ions may or may not be produced, depending on how $E_{kinetic}$ compares with the binding energy in the ion (E_b). Na^+ ions will be produced whenever $E_{kinetic} > E_b$. Otherwise, only NaI^+ will be formed.

In region III, the electron energy will increase as the kinetic energy of the atoms decreases when heading to the outer turning point of the potential. At 8.7 Å, zero kinetic energy electrons are emitted from energy conservation. $E_{kinetic}$ is large, and therefore, the ions produced will dissociate and give rise to the Na^+ signal. As the internuclear distance increases, i.e., as the wave packet moves in time toward the outer turning point, $E_{kinetic}$ decreases and the energy of the ejected electron increases. Near the turning point, the relative kinetic energy of the nuclei vanishes. All the available energy is imparted to the outgoing electron, leaving the NaI^+ ion with so little internal energy that this ion will survive and be detected as NaI^+.

However, another important assumption has to be made. In agreement with the experimental fact that no signal is observed around the inner turning point, i.e., in region I, we must assume that the absolute ionization cross section in the Na^+I^- region is a lot greater than the ionization cross section of the covalent NaI region. In the covalent region of the A state the molecule can be considered as a van der Waals complex where the sodium atom is weakly perturbed. Thus, the ionization cross section in this region should be very similar to the Na atomic ionization cross section, which is on the order of $\sigma_{Na} = .1$ Mb.[22,23] In the ionic region of the A state, the interatomic distance is such that, in a first approximation, the ionization process can be considered as the photodetachment of the electron from the I^- anion. The absolute photodetachement cross section of I^- is on the order of 20 Mb in the 4−5 eV energy region.[24] Therefore, the NaI ionization cross section should be ∼200 times greater in the ionic Na^+I^- region than in the covalent region.

With these simple assumptions, the results can be simulated using classical mechanics. At time $t = 0$, the particles are promoted to the excited NaI potential, with an initial energy corresponding to the difference between the energy of the pump laser and the binding energy of the A state. The movement is calculated by resolving Newton's equations with a Runge−Kutta integrator. At each time (or distance), the energy of the electron and the kinetic energy of the atoms in the ionic potential can be calculated. If $R > 8.7$ Å (the crossing point between the dressed excited state and the ionic state, C_2 in Figure 5), $E_{electron}$ becomes positive and ions are produced. For each distance, the kinetic energy $E_{kinetic}$ is compared to the binding energy in the ion. If $E_{kinetic}$ is smaller than the binding energy, then NaI^+ is observed, and if $E_{kinetic}$ is larger than the binding energy, Na^+ ions are produced. Running the trajectory produces *square* functions of time that tell us when and where Na^+ and NaI^+ are produced. To mimic the fact that the laser pulses are not infinitely narrow and that the wave packet is spread in time/distance, these functions are convoluted with a Gaussian function of a given width.

With this very simple model, a remarkable agreement between simulation and data is obtained for the ion signals as a function of time, as shown in parts a and b of Figure 6, for an excitation wavelength of 312 nm. If the NaI^+ signal (width 300 fs) is used to fit the width of the Gaussian function (the best fit was

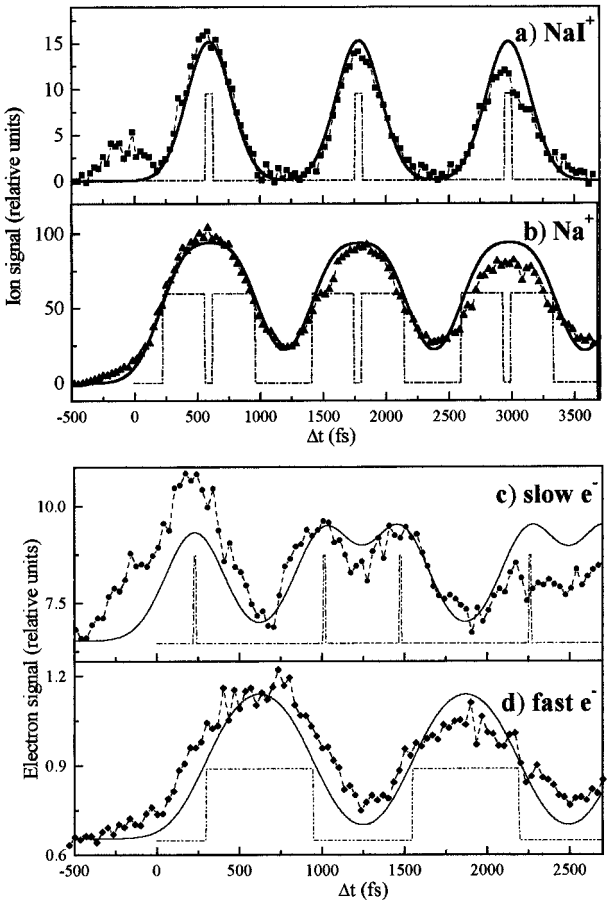

Figure 6. Comparison between model and experiment for $\lambda_1 = 312$ nm. (a, b) simulation of the ion signals. The dotted line shows the square function issued from the classical dynamic simulation. The decrease of the signal due to the avoided crossing in the A state is not taken into account. The full line is a convolution of the first curve by a Gaussian function with a width of 250 fs. The vertical scale corresponds to the simulation. The calculated Na^+/NaI^+ ratio is found to be 6. Data represented by ■ are experimental points. The relative intensity of the experimental points has been normalized to the calculated ones. (c, d) simulation of the photoelectron signal. Slow electrons are taken from 0 to 500 cm^{-1} in the classical dynamic simulation and convoluted by the same Gaussian function as for the ion signal (width of 250 fs). Fast electrons are taken from 2000 cm^{-1} to the maximum energy possible of ~3400 cm^{-1}. The dotted line shows the classical dynamic simulation. The full line shows the convolution of the simulation by a Gaussian function with a width of 250 fs. Experimental points are for fast electrons (◆) and for slow electrons (●). In this case, since the experimental signal is not corrected for detection efficiency, the relative intensity of the simulated curves has been normalized to the intensity of the experimental points.

obtained for a width of 250 fs), then the Na^+ signal is simulated with the correct contrast and width. The Na^+/NaI^+ ratio is only qualitatively reproduced giving a 6/1 ratio, whereas the observed ratio is higher than 10/1. The spectra obtained at another pump wavelength (347 nm) have also been simulated. The contrast between successive Na^+ peaks is greater at this wavelength; the peak width is 320 ± 50 fs, whereas it is 460 ± 50 fs at 312 nm with a shorter laser pulse. This reflects the evolution of the wave packet at different energies. At lower energy, the wave packet spends less time in the ionic part of the potential, and the time window viewed through ionization is shorter. This decrease in the peak widths is reproduced well in the simulation.

A similar simulation can be performed for the electrons by dividing the continuous electron spectrum generated by the model into two parts: electrons with less than 500 cm^{-1} of energy and electrons with more than 2000 cm^{-1} of energy. Here again, the simulated spectra resemble the experimental ones (see parts c and d of Figure 6).

The very simple model proposed here is based on the same assumptions as that for the wave packet calculations on the time evolution of ion signals performed by Engel and Metiu,[14] which, however, deserve some comments. Their calculations indicate that the Na^+ fragment is obtained when the wave packet is in the region of the ionic curve, which is in complete agreement with our results. But they did not predict the appearance of NaI^+ at the outer turning point, where the ejected photoelectron leaves with all the available energy. It was rather unexpected that NaI^+ ions only bound by a few wavenumbers would be detected. The calculations also predicted that the NaI^+ signal should be mainly observed at short distances around the equilibrium distance in the ionic state where the ion is strongly bound, assuming a good Franck−Condon (FC) overlap between the covalent region of the A state and the ionic state. This is not observed experimentally, and the reason must be that the FC factors are not large enough to counterbalance the poor ionization efficiency in the covalent region as compared to the ionization efficiency in the ionic part of the A state.

The same comments can be made about the calculations of the photoelectron spectrum published by Braun, Meier, and Engel.[15] The present work is partially in agreement with these calculations; high-energy electrons are indeed observed when the wave packet reaches the outer turning point, and as already stated, these high-energy electrons partly lead to stable NaI^+ ions. Some discrepancies are observed for low-energy electrons. In agreement with the calculations, only a few low-energy electrons are emitted at the outer turning point, but the authors suggest that low-energy electrons are emitted mostly when the wave packet is in the covalent region ($R < 6$ Å). The spectra recorded here show that slow electrons are emitted with a delay of 200 ± 40 fs, which from a classical dynamic simulation corresponds to $R \approx 8 \pm 1$ Å, in the ionic−covalent crossing region, i.e., at longer distances than predicted. Once again, the difference between calculations and experiment comes from the ionization efficiency (or transition dipole moment), which is set as independent of the internuclear distance in the calculations. Clearly, this hypothesis has to be refined and more sophisticated calculations would be necessary.

A last point to be mentioned concerns the observation of "negatively" delayed peaks on the NaI^+ channel (Figure 3) and on the slow electrons (Figure 4). Negative delays mean that the pump and probe lasers are reversed, i.e., the pump laser is the 263 nm laser and the probe the 312 nm laser. This excitation scheme is only seen once, and no recurrences at longer times are observed.

For the NaI^+ channel 1, this signal at −90 ± 50 fs may be due to the excitation of the $\Omega = 1$ state (which corresponds to the same $Na(^2S_{1/2}) + I(^2P_{3/2})$ limit as the A $\Omega = 0$ state). The $\Omega = 1$ state is optically accessible from the ground state but has a different symmetry; there is no interaction between states and no avoided crossing, and $\Omega = 1$ rapidly dissociates.[2,25] However a nonresonant photoionization process can also occur at $t = 0$. Such a process could be hidden under the observed signal.

For slow electrons, the negative peak arrives at −180 ± 50 fs and may correspond to the Na_2I^+ ions present in the mass spectra; the time evolution of the Na_2I^+ signal presents a peak at −200 ± 60 fs, and the signal drops to zero at longer delays. The origin of the Na_2I^+ signal has not been elucidated at present.

Conclusion

In this experiment we have shown that wave packet dynamics can be followed by direct ionization to the dissociation/ionization

continua. The branching ratio between dissociative ionization and ionization toward a stable molecule can be understood using very simple classical mechanics arguments. This paper shows that, in this case, the ionization efficiency is greatly enhanced when the molecule has a strong ionic character. A theoretical treatment to account for this observation is highly desirable.

Acknowledgment. The authors thank A. Suzor, E Charon, A. Keller, and Ph. Millié for helpful discussion. The authors are indebted to B. Tardivel, O. Sublemontier, and P. Ceraolo for their help in setting up the NaI ovens.

References and Notes

(1) Rosker, J.; Rose, T. S.; Zewail, A. H. *Chem. Phys. Lett.* **1988**, *146*, 175.

(2) Rose, T. S.; Rosker, J.; Zewail, A. H. *J. Chem. Phys.* **1989**, *91*, 7415.

(3) Cong, P.; Mokhtari, A.; Zewail, A. H. *Chem. Phys. Lett.* **1990**, *172***,** 109.

(4) Zewail, A H. *Femtosecond chemistry*; Manz, J., Wöste, L., Eds.; VCH Verlagsgesellschaft: Weinheim, 1994; p 15.

(5) Materny, A.; Herek, J. L.; Cong, P.; Zewail, A. H. *J. Phys. Chem.* **1994**, *98*, 3352.

(6) Herek, J. L.; Materny, A.; Zewail, A. H. *Chem. Phys. Lett.* **1994**, *228***,** 15.

(7) Cong, P.; Roberts, G.; Herek, J. L.; Mohkatari, A.; Zewail, A. H. *J. Chem. Phys*. **1996**, *100*, 7832, and references therein.

(8) Motzkus, M.; Pedersen, S.; Zewail, A. H. *J. Phys. Chem.* **1996**, *100*, 5620.

(9) Zewail, A. H. *Femtochemistry*; World Scientific: Singapore, 1994; Vols. 1 and 2.

(10) Gruebele, M.; Zewail, A. H. *J. Chem. Phys.* **1993**, *98*, 883.

(11) Baumert, T.; Thalweiser, R.; Weiss, V.; Gerber, G. *Femtosecond chemistry*; Manz, J., Wöste, L., Eds.; VCH Verlagsgesellschaft: Weinheim, 1994; p 397, and references therein.

(12) Blanchet, V.; Bouchène, M. A.; Cabrol O.; Girard, B. *Chem. Phys. Lett.* **1995**, *233*, 491.

(13) Krim, L.; Qiu, P.; Halberstadt, N.; Soep, B.; Visticot, J. P. In *Femtosecond chemistry*; Manz, J., Wöste, L., Eds.; VCH Verlagsgesellschaft: Weinheim, 1994.

(14) Engel, V.; Metiu, M. *Chem. Phys. Lett.* **1989**, *77*, 155,

(15) Braun, M.; Meier, C.; Engel, V. *J. Chem. Phys.* **1996**, *105***,** 530.

(16) Mestdagh, J. M.; Berdah, M.; Dimicoli, I.; Mons, M.; Meynadier, P.; D'Oliveira, P.; Piuzzi, F.; Visticot, J. P.; Jouvet, C.; Dedonder-Lardeux, C.; Martrenchard, S.; Soep, B.; Solgadi, D. *J. Chem. Phys.* **1995**, *103*, 1013.

(17) Faist, M. B.; Levine, R. D. *J. Chem. Phys.* **1976**, *64*, 2953.

(18) Bower, R. D.; Chevrier, P.; Das, P.; Foth, H. J.; Polanyi, J. C.; Prisant M. G.; Visticot, J. P. *J. Chem. Phys.* **1988**, *89***,** 4478.

(19) Schaefer, S. H.; Bender, D.; Tiemann, E. *Chem. Phys.* **1984**, *64*, 89.

(20) Chapman, S.; Child, M. S. *J. Phys. Chem.* **1991**, *95*, 578.

(21) Sterling, M.; Zadoyan, R.; Apkarian, V. A. *J. Chem. Phys.* **1996**, *104*, 6497.

(22) Hudson R. D.; Carter, V. L. *J. Opt. Soc. Am.* **1967**, *57*, 651.

(23) Aymar, M. *J. Phys. B.: At. Mol. Phys.* **1978**, *11*, 1413.

(24) Radojevic, V.; Kelly, H. P.; Johnson, W. R *Phys. Rev. A.* **1987**, *35*, 2117.

(25) Berry, R. S. *Alkali Halide Vapors*; Davidovits, P., McFadden. D. L., Eds.; Academic: New York, 1979.